JOURNAL OF MATERIALS SCIENCE 21 (1986) 3966–3976

The influences of sulphur and phosphorus additions on the creep cavitation characteristics in type 304 stainless steels

JUN HWA HONG*, SOO WOO NAM,
Department of Materials Science and Engineering, Korea Advanced Institute of Science and Technology, PO Box 131, Cheongryang, Seoul, Korea

SUN PIL CHOI
Reactor Materials Department, Korea Advanced Energy Research Institute, PO Box 7, Daeduk-Danji, Choong-Nam, Korea

The effects of impurities on creep cavitation characteristics in type 304 stainless steels with and without additions of sulphur and/or phosphorus have been studied using four experimental heats. Over a limited range of stress at 1000 K, the change in size distribution of creep cavities and carbide precipitates, and the level of impurity segregation with the amount of addition have been investigated. It is found that phosphorus accelerates the nucleation of creep cavities, but retards the growth of them. However, sulphur had little effect on both nucleation and growth of the cavities. It has also been found that ageing prior to testing inhibits creep cavitation. The effects of impurities on cavitation are analysed and discussed from the viewpoint of the change in the segregation of impurities and the precipitation of carbides due to impurity additions.

1. Introduction

Imputities in metals and alloys are known to influence the mechanical properties, especially if they segregate at the grain boundary and free surfaces. Phenomena such as temper embrittlement [1] intergranular corrosion cracking [2] and hydrogen embrittlement [3] are subject to impurity induced or assisted grain boundary decohesion at relatively low temperature. Thus one tends to expect deleterious effects by impurities even on creep and creep fracture. However, a big difference between the mechanisms of low (temper embrittlement) and high temperature fracture (creep embrittlement) makes it difficult to take such a conclusion for granted.

While the findings by various investigators [4–8] show that creep and cavitation of certain alloy steels are affected by certain impurities, no consistent picture has emerged to date. Furthermore, the exact mechanisms responsible for the effects of impurity segregation at grain boundaries and cavity surfaces on creep cavitation are not well understood. And there have been few direct observations of segregated impurities in cavitated alloys and the details of such segregation and its effects on creep cavitation and high temperature fracture have not been thoroughly studied. It has only been proposed that such segregation could affect the degree of cavitation through its effects on the parameters such as grain boundary energy, surface energy and diffusivity, which control the nucleation and growth of creep cavity [9–11]. In particular, little is known about the interaction between segregation and grain boundary precipitation and their combined effects on creep cavitation.

In this investigation, the creep cavitation characteristics of typical type 304 stainless steels, without and with sulphur and/or phosphorus additions, will be considered. The reason why austenitic stainless steels were chosen is the following. Most of the investigations on the effects of impurity have been concentrated on low alloy ferritic steels and copper. On the other hand, few investigations have been conducted for austenitic stainless steels such as type 304, which are mainly used under creep conditions. Previous reports show that segregation of some impurities such as phosphorus and sulphur at grain boundaries is known to enhance stress corrosion cracking susceptibility [2] and to cause temper embrittlement [12, 13], and that some impurities like phosphorus also segregate at surfaces and grain boundaries during irradiation [14, 15].

The principal aim of the present work is to investigate the effect of sulphur and/or phosphorus on the creep cavitation of the type 304 stainless steels. For this, we have prepared four different groups of alloys such as commercial grade type 304 stainless steel, sulphur and/or phosphorus doped ones. The significant role of the impurities for the stages of nucleation and growth of creep cavity will be discussed.

Present address: Reactor Materials Department, KAERI, PO Box 7, Daeduk-Danji, Choong-Nam, Korea.

0022–2461/86 $03.00 + .12

TABLE I Chemical composition of commercial, sulphur-, phosphorus-, sulphur, phosphorus doped type 304 stainless steels studied

Material	Composition (wt %)											Composition (p.p.m)		
	C	S	P	Cr	Ni	Si	Mn	Mo	V	Cu	Co	H	N	O
C,1 (commercial)	0.057	0.018	0.033	18.32	8.64	0.36	0.81	0.16	0.06	0.17	0.13	1.24	454	249
S,2 (S-doped)	0.059	0.055	0.032	18.52	8.32	0.39	0.94	0.15	0.07	0.15	0.13	1.13	402	198
SP,3 (S, P-doped)	0.052	0.060	0.143	18.25	8.35	0.38	0.89	0.16	0.07	0.17	0.12	1.58	493	134
P,4 (P-doped)	0.058	0.018	0.160	18.25	8.36	0.41	0.82	0.16	0.07	0.15	0.12	1.45	506	129

2. Materials and experimental procedures

2.1. Materials

Four experimental heats based on a commercial grade type 304 stainless steel have been produced in an induction furnace with compositions shown in Table I. The ingots were forged and then hot rolled to 10 mm thickness plate. Prior to machining the steels were solution annealed at 1373 K for 1 h followed by a water quench. The average grain size of the materials was 90 $\pm$ 10 μm.

2.2. Creep test

Tensile creep specimens with 3.2 mm diameter and 25 mm gauge length were machined. To avoid the gradual carbide precipitation during creep test, the specimens were aged before test at 1023 K for 100 h to allow well defined grain boundary carbide precipitations that were stable during subsequent creep cavitation experiments. In some cases, specimens were tested as solution annealed (SA) condition and observed for the cavitation behaviour in order to be compared with that of aged samples.

Creep tests were conducted in air in creep testing machine equipped with an Andrade-Chalmers constant stress arm. Test temperature was kept constant within $\pm$1 K using a split type furnace and creep strain was continuously recorded through measuring by a linear variable differential transducer (LVDT) with an accuracy of 4×10^{-5} sec^{-1}.

Specimens, having mirror-like surfaces are tested in the temperature range of 1000 K ($\sim 0.6\,T_m$) and under the stress range of 75 $\sim$ 150 MPa (applied stress normalized with elastic modulus, $\sigma/E = 5 \times 10^{-4} \sim 1 \times 10^{-3}$). At each test condition, every test was performed and terminated at various predetermined times or strains by cooling to room temperature, with argon gas, under stress. But some of the specimens were tested up to fracture.

2.3. Assessment of cavitation damage

The shape, size and the amount of intergranular creep cavities, which were nucleated and grown during the creep test, were examined first by the cryogenic impact fracture technique, which can be widely used to reveal the shape and size of the creep cavities on the fracture surface.

The second technique is metallographic observation of the longitudinally sectioned surface followed by polishing and etching in a solution of 8 HNO_3, 54 HCl in water. This technique has an advantage of the investigation of the inter- and intragranular precipitates simultaneously with the creep cavities. However, no importance can be attached to the shape or to the size of these cavities as they may have been distorted by the sectioning and polishing processes.

Approximately five grains with the boundary area normal to the stress axis were investigated for each fractured specimen to determine the size distribution of the creep cavities with a scanning electron microscope (SEM).

2.4. Microstructural observation

The sizes and density of inter- and intragranular precipitates were determined by the examination of polished and etched sections in SEM, and of thin foils and carbon extraction replicas in transmission electron microscope (TEM) at 160 kV. The precipitates were identified by the selected area diffraction pattern.

A PHI model 590 scanning Auger microprobe (SAM) was used for impurity segregation analysis. Samples for SAM were machined from the middle section of the crept specimens and fractured at low temperature under ultrahigh vacuum conditions. Auger spectra and phosphorus, sulphur Auger maps were obtained from several grain boundaries and cavity surfaces.

Quantitative analyses of Auger spectra were based on relative sensitivity factors from published standard spectra of pure elements [16]. Impurity segregation levels were measured as peak-height-ratios (PHR) using the $Fe_{703\,eV}$ peak for normalization and at %. The following Auger peaks were measured: $P_{120\,eV}$, $S_{152\,eV}$, $C_{272\,eV}$, $Cr_{529\,eV}$ and $Ni_{848\,eV}$.

3. Experimental results

3.1. The characteristics of cavitation

Typical creep cavities on intergranular surfaces revealed by fracture at liquid nitrogen temperature, are shown in Fig. 1. Cavities are predominantly in the form of round-type, distributed heterogeneously on the grain boundaries, and located preferentially on bundaries that are approximately normal to the stress axis and on twin interfaces, as shown in Fig. 1a. Cavities are densely nucleated in the region of triple points, where extensive cavity coalescences are frequently found in Figs 1a and b, resulting in a wedge-like cavity. Fig. 1c shows the well grown cavities, which are associated with intergranular precipitates as in other engineering alloys [17]. Geometry and position of cavities are clearly shown in the paired surfaces of Fig. 1d.

Another examination of such cavities by the metallographic sectioning technique shows that creep cavities are preferentially nucleated and grown at the interfaces of the grain boundary precipitates, as shown in Fig. 2. These may support the idea that the cavitation characteristics may be influenced by the

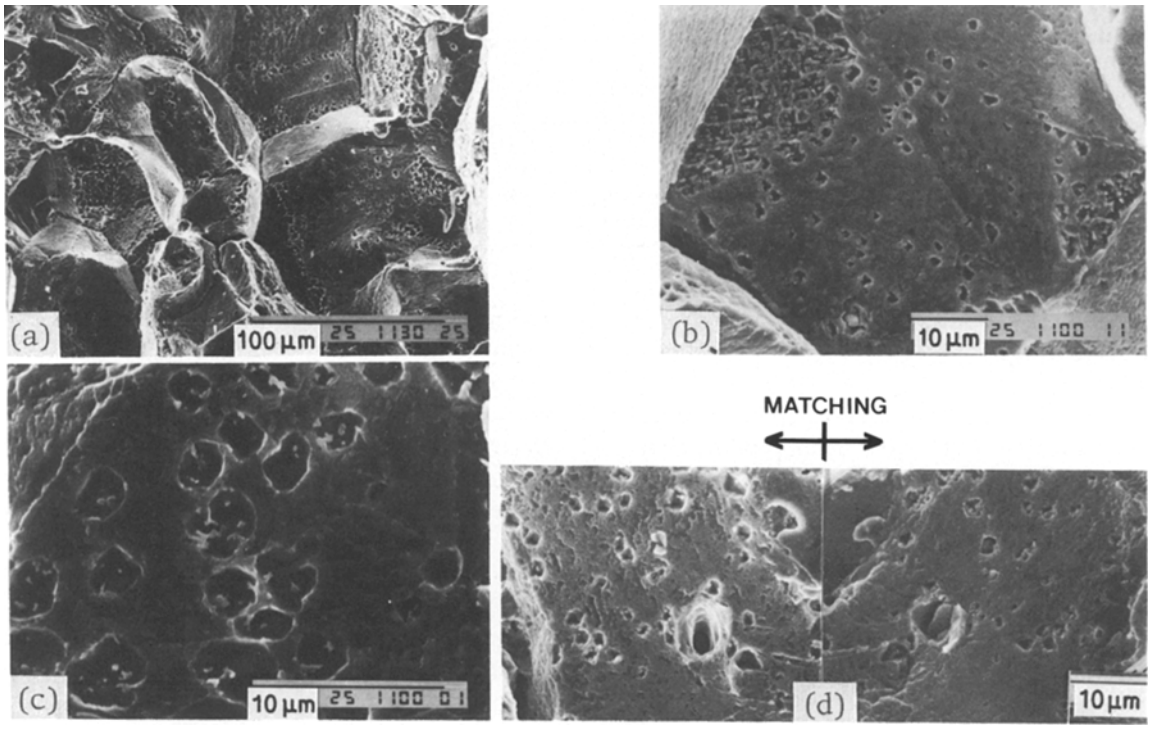

Figure 1 Typical SEM micrographs of creep cavities on intergranular fracture surface: (a) macroscopic view; (b), (c) locally coalesced and well-grown cavities in crept C,1 steel; (d) cavities on two matching surfaces in crept S,2 steel.

boundary second phase particles. Round-type cavities are also predominantly found even in the specimen tested with the condition of high stress of 150 MPa at 1000 K, in which wedge-type cavities are expected to be formed.

Fig. 3 shows the difference in the extent of creep cavitation for the solution annealed steels crept at 1000 K and 100 MPa for the same creep time of 3.5×10^5 sec. It can be observed that there exists large amounts of cavities which are relatively large in size in the phosphorus-free steels such as C,1 and S,2 whereas they are small in size and numerous in phosphorus-added steels such as SP,3 and P,4.

Cavity size distribution measured by cryogenic fracture technique, averaged over the grain boundary area normal to the stress axis, is shown in Fig. 4. For C,1

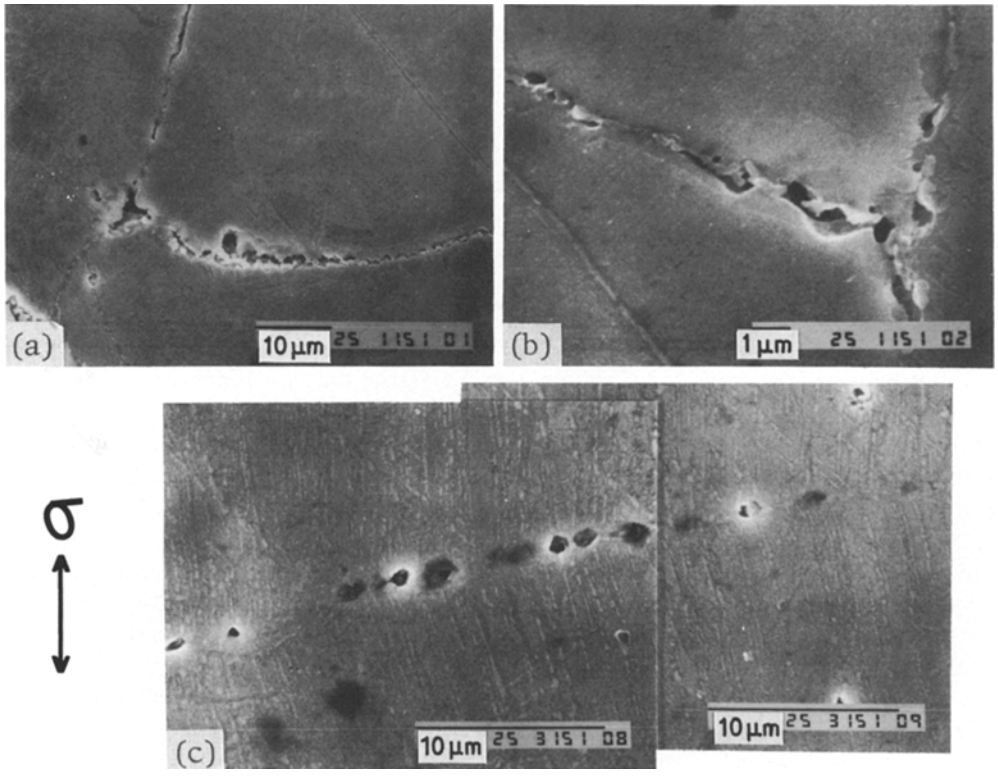

Figure 2 Typical SEM micrographs of longitudinally polished and etched sections of aged and crept (1000 K, 150 MPa, 3.5×10^5 sec) specimens showing cavities formed at the interfaces of the grain boundary precipitates. (a) (b) C,1 (c) SP,3.

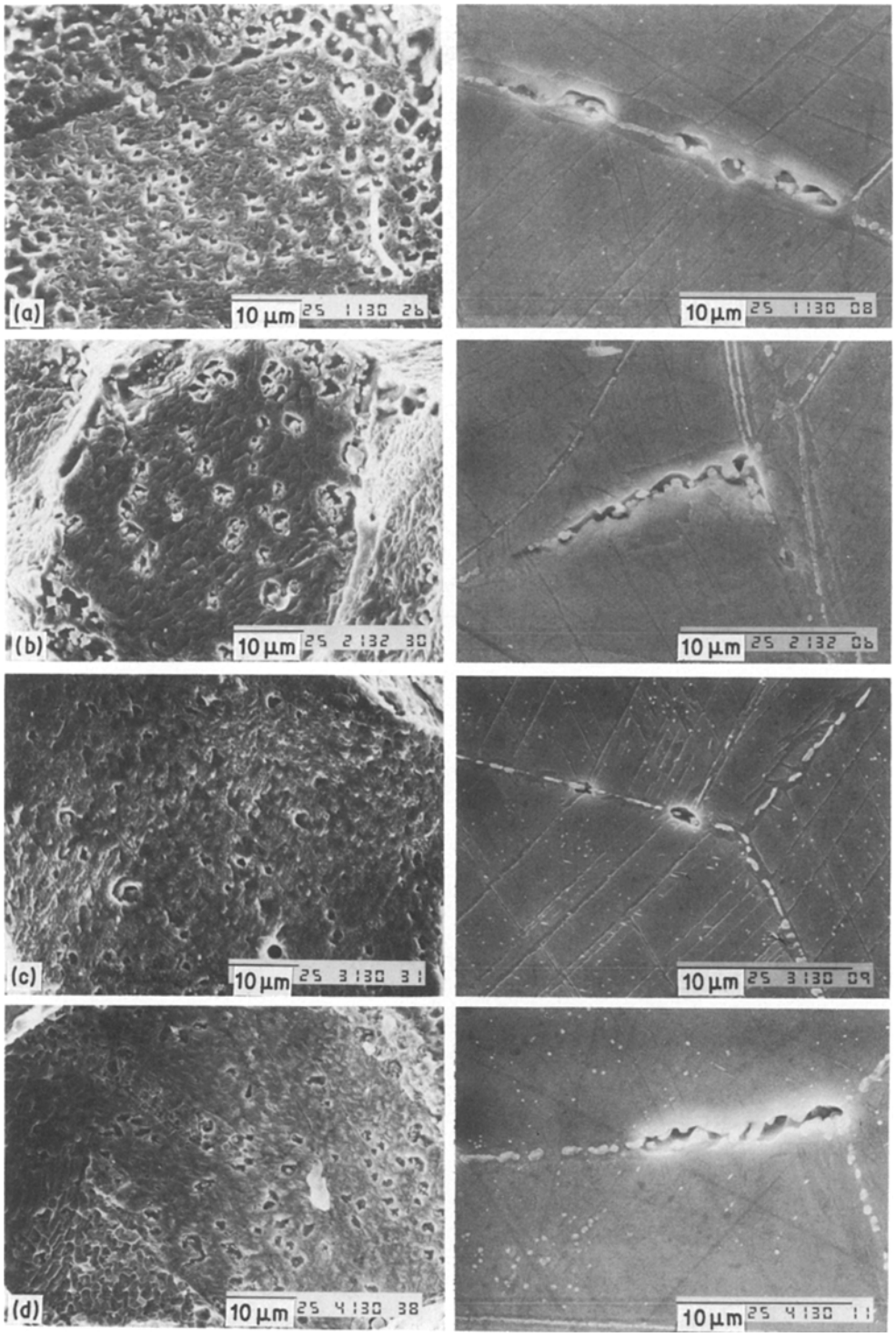

Figure 3 Cavities in solution annealed specimens crept at 1000 K, 100 MPa for 3.5×10^5 sec. Left micrograph is obtained by cryogenic fracture technique, right by metallographic sectioning technique. (a) C,1, (b) S,2, (c) SP,3, (d) P,4.

and S,2 steels (phosphorus-free steels) cavity density gradually decreases with cavity diameter. On the other hand, for SP,3 and P,4 steels (phosphorus-added steels) cavity size distributions are shifted to the side of the smaller cavity. Fig. 4 also shows that solution annealed steels have a slightly higher tendency in cavitation than that of aged steels.

Figs 5 and 6 show the change in the size distribution of cavities with creep time for aged and solution annealed steels, respectively. The figures inside the left corner of the figure represent the cavity density with the range of $0.25 \sim 0.5\,\mu$m in diameter for corresponding creep time, respectively. It can be shown that cavities are continuously nucleated with creep deformation and that cavities grow as creep deformation proceeds. Impurity effects on nucleation and growth of creep cavities can be deduced from the basis of the above mentioned cavity size distribution of Figs 4 to 6.

Generally the number of cavities per unit grain boundary area is linearly related to the time dependent creep strain. That is, cavities are believed to be nucleated continuously with creep strain [18–20]. Accordingly, the extent of cavitation per unit creep strain can be a measure to assess the cavity nucleation.

Figs 7 and 8 show the cavity size distribution

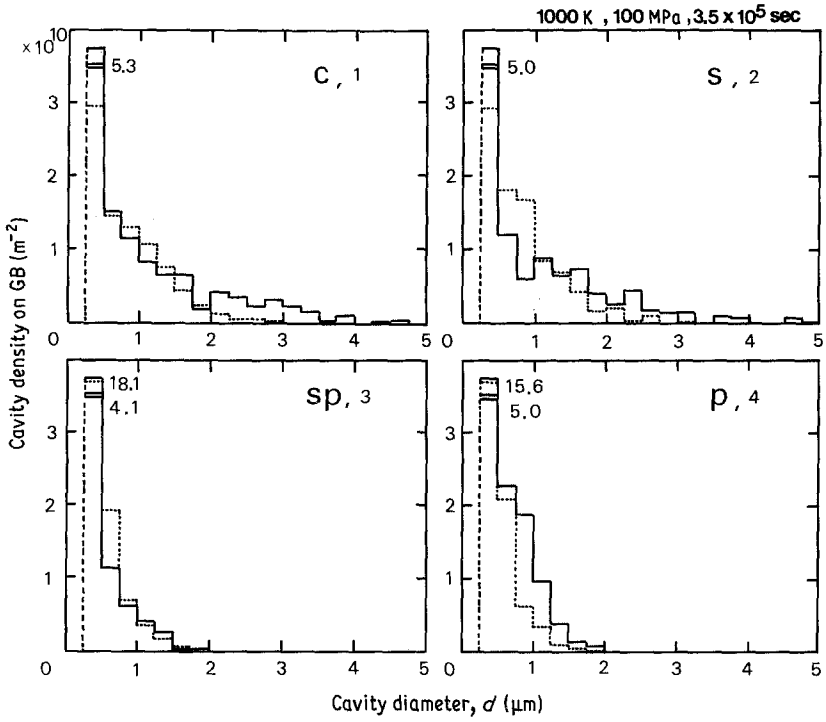

Figure 4 Cavity size distributions in aged and solution annealed specimens crept at 1000 K, 100 MPa for 3.5 × 10^5 sec. (– – –) aged; (——) SA.

normalized by 1% creep strain for aged and solution annealed steels, respectively. As it would be expected from Figs 4 to 6, Figs 7 and 8 also indicate the similar tendency to cavitation due to impurity.

Cavity nucleation factors per unit grain boundary area per 1% creep strain, P, which correspond to the area under cavity size distribution curve of Figs 7 and 8, are summarized in Table II. It is seen that those steels with phosphorus have a markedly increased number of cavities, i.e. the cavity nucleation factors of the phosphorus-added steels are 4 to 5 times larger compared with those of the phosphorus-free steels. It is also found that the factor is slightly increased for solution annealed steels than for aged steels.

In order to assess cavity growth rate, the ith largest cavity diameter method described elsewhere [18] is used. In the present work, the growth rate is estimated on the basis of the diameter of the 2500th largest cavity per mm^2 in brain boundary area normal to the stress axis.

By checking the variation of the diameter of the ith largest cavities, d_i, with creep time, t, at 1000 K and 100 MPa, as shown in Fig. 9, it was found that the cavity diameter is increased linearly with creep time during secondary creep.

Measured growth rates of creep cavities are shown in Table III. In contrast to cavity nucleation, the growth rates of creep cavities in the phosphorus-added aged steels become 4 to 5 times smaller than those in the phosphorus-free aged steels. The increase of 2 to 3 times in growth rates of solution annealed steels is also observed.

From the above investigations, the following effects of impurity on nucleation and growth of creep cavities

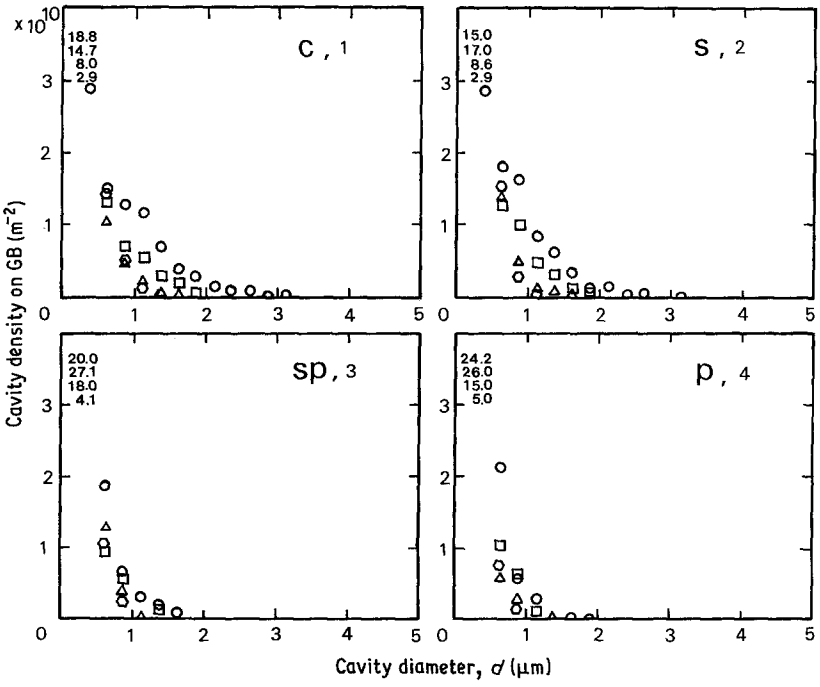

Figure 5 Variation of cavity size distribution with creep time in aged and crept (1000 K, 100 MPa) specimens. (○) 4.3 × 10^4; (△) 8.6 × 10^4; (□) 1.7 × 10^5; (○) 3.5 × 10^3 sec.

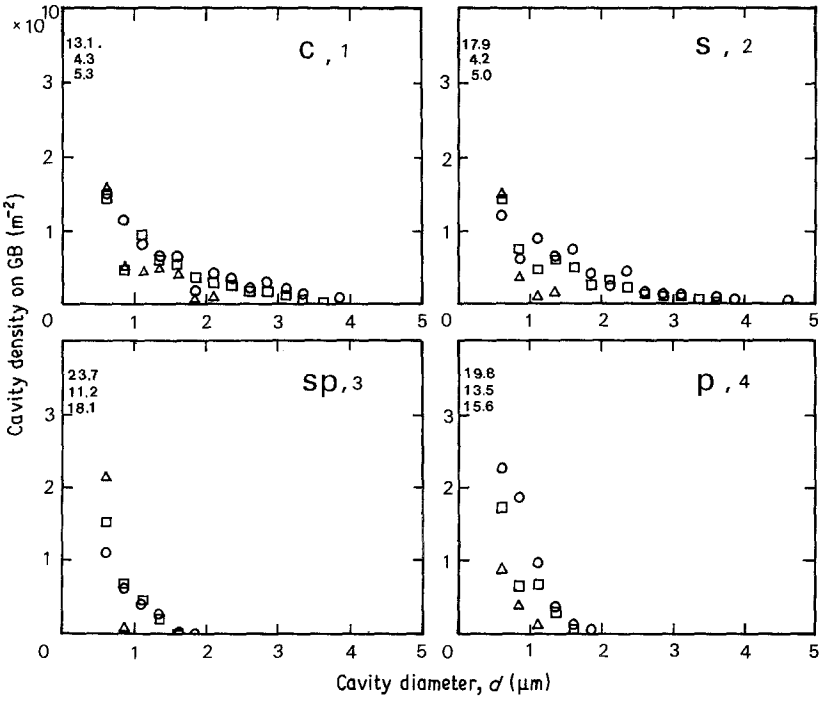

Figure 6 Variation of cavity size distribution with creep time in solution annealed and crept (1000 K, 100 MPa) specimens. (△) 8.6×10^4; (□) 1.7×10^5; (○) 3.5×10^5 sec.

can be deduced. Phosphorus-added steels show the higher nucleation rate and the lower growth rate of creep cavities than in phosphorus-free steels. Accordingly, it can be evaluated that small amounts of phosphorus addition are very effective in accelerating cavity nucleation, and in retarding cavity growth. However, there is no big difference in cavitation between C,1 and S,2 steel and SP,3 and P,4 steel. This fact reflects that sulphur has a little effect on the cavitation characteristics. On the other hand, solution annealing prior to creep testing causes a greater increase in the rates of nucleation and growth of creep cavities than ageing does.

These effects of impurities may be attributed to the difference in the level of segregation at the grain boundaries and cavity surfaces and in the precipitation behaviour of intergranular carbides.

3.2. Microstructural observation

TEM micrographs taken from thin foils of crept specimens tested at 1000 K and 100 MPa for 3.5×10^5 sec are shown is Fig. 10. It can be observed that more precipitates are finely distributed in the matrix in the phosphorus-added steels than in the phosphorus-free steels. The precipitates were identified as $M_{23}C_6$-type carbide, which contains mainly chromium, iron and nickel, by analysis of selected area diffraction patterns. Fig. 10 also shows the dislocation morphology which is formed during creep deformation.

The carbides are more clearly illustrated by TEM photographs taken from carbon extraction replicas of the same specimens as in Fig. 11. It was found that there is a difference in the extent of the intragranular carbides, which have been related to the phosporus addition (not to the sulphur addition), and that addition of phosphorus affects the size, spacing and density of carbides.

Table IV summarizes the information about the inter- and intragranular carbides obtained from TEM and SEM observations. It can be found that the presence of phosphorus affects the precipitation of carbides, which is consistent with other papers [21–23], and that there is a difference in carbides between solution annealed and aged steels.

Impurity segregration at grain boundary and cavity surface of crept specimen is illustrated in Fig. 12. The left column of Fig. 12 shows the secondary electron image of the grain boundary facet obtained while the specimen was still in the Auger electron spectroscopy (AES) chamber. The sample was for SP,3 steel aged and crept at 1000 K and 100 MPa for 3.5×10^5 sec.

Fig. 12 also shows the Auger maps for phosphorus and sulphur over the same field of view as in secondary electron image. The maps indicate that phosphorus and/or sulphur were segregated at grain boundaries and cavity surfaces, and that the sulphur-enriched areas on the surface were generally located at MnS inclusions which are precipitated at the grain boundaries prior to cavitation.

Auger spectra from points 1, 2 and 3 of the secondary

TABLE II Cavity nucleation factor per unit grain boundary area per 1% creep strain

Material	Cavity nucleation factor, P(m^{-2} per 1% ε_c)	
	Aged	SA
C,1	1.29×10^9	1.97×10^9
S,2	1.23×10^9	1.62×10^9
SP,3	4.64×10^9	5.60×10^9
P,4	6.24×10^9	7.96×10^9

TABLE III Measured growth rate of creep cavity

Material	Cavity growth rate G($msec^{-1}$)	
	Aged	SA
C,1	3.33×10^{-12}	7.34×10^{-12}
S,2	3.27×10^{-12}	7.16×10^{-12}
SP,3	0.90×10^{-12}	3.54×10^{-12}
P,4	0.67×10^{-12}	2.36×10^{-12}

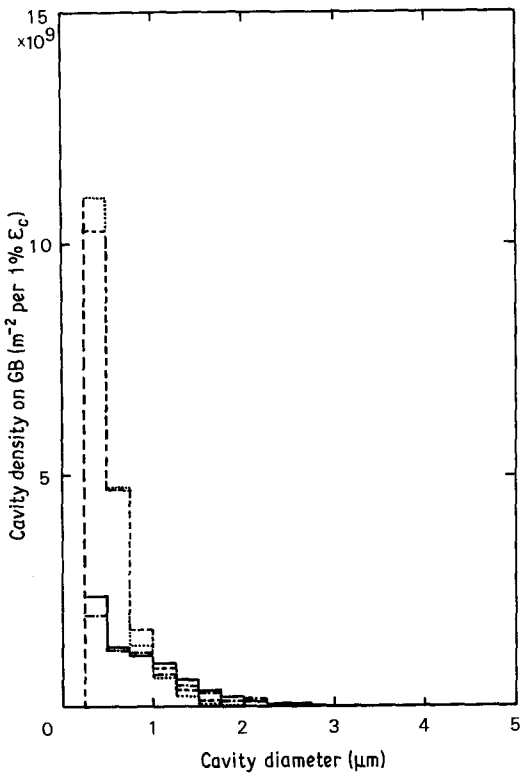

Figure 7 Dependence of the cavity density per 1% creep strain on the cavity diameter in aged and crept (1000 K, 100 MPa) specimens. (——) C,1; (–·–) S,2; (– – –) SP,3; (····) P,4.

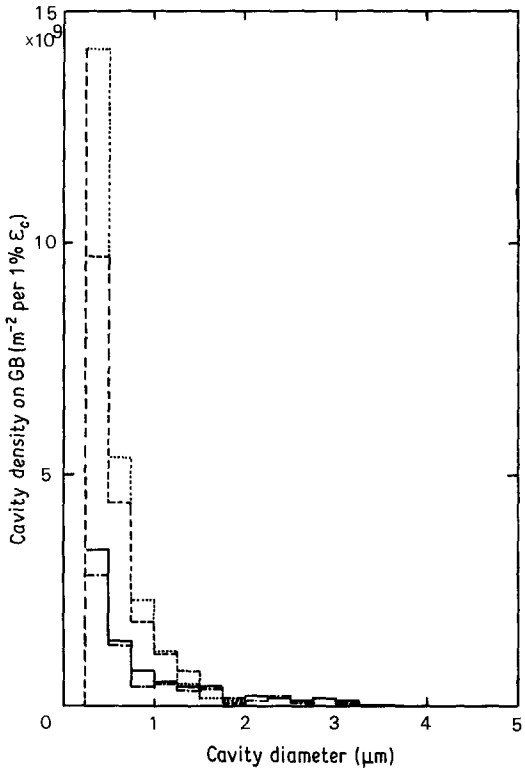

Figure 8 Dependence of the cavity density per 1% creep strain on the cavity diameter in solution annealed and crept (1000 K, 100 MPa) specimens. (——) C,1; (–·–) S,2; (– – –) SP,3; (····) P,4.

electron image are also shown in Fig. 12. Faceted flat grain boundary area of point 1 shows the large peak for phosphorus, which indicates that phosphorus is segregated at the grain boundary. The large sulphur signal from the cavity surface containing MnS inclusion of point 2 is observed, whereas, general segregation of phosphorus and sulphur at the cavity surface is also obtained.

Auger peak height ratio normalized by $Fe_{703\,eV}$ peak and at % for phosphorus and sulphur are summarized in Table V. Phosphorus segregation at grain boundary and sulphur and rather slight phosphorus segregation at cavity surface can be characterized.

Such impurity segregations to grain boundary and cavity surface will directly influence the cavity nucleation and growth kinetics through their effects on the interfacial energy and diffusivity.

Although Fig. 12 shows only the AES result of SP,3 steel, other steels showed similar impurity segregation behaviour.

4. Discussion

4.1. Impurity effects on cavity nucleation

A study of cavity nucleation has been conducted by observing the effect of impurities on the nucleation in a commercial grade type 304 stainless steel. The critical cavity size is far smaller than the limit of resolution of our experimental technique. Therefore, it has to be borne in mind that initial stage of growth may be involved in evaluating nucleation of creep cavities. In

TABLE IV The size ($\bar{d}$), spacing (λ) and density (N_a) of carbide on the grain boundary and grain matrix

Material		Intergranular carbide				Intragranular carbide		
		$\bar{d}$ (μm)	λ (μm)	$\bar{d}/\lambda$	N_a (m^{-2}, × 10^{12})	$\bar{d}$ (μm)	λ (μm)	N_a (m^{-2}, × 10^{11})
SA + aged*	C,1	0.51	0.66	0.77	2.51	0.10	116	1.09
	S,2	0.47	0.72	0.65	2.63	0.11	120	0.96
	SP,3	0.54	0.71	0.76	2.20	0.12	39.8	2.66
	P,4	0.55	0.77	0.71	2.04	0.10	29.9	4.25
Aged* + crept**	C,1	0.63	0.94	0.67	1.48	0.12	52.8	1.98
	S,2	0.60	0.93	0.65	1.59	0.11	75.9	1.51
	SP,3	0.80	0.97	0.82	1.06	0.12	27.0	3.82
	P,4	0.75	0.90	0.83	1.21	0.11	19.2	5.81
SA + crept**	C,1	0.45	0.73	0.62	2.74	0.07	58.8	3.09
	S,2	0.42	0.71	0.59	3.06	0.07	51.5	3.53
	SP,3	0.55	0.70	0.79	2.18	0.05	34.3	7.41
	P,4	0.55	0.77	0.71	2.03	0.06	31.0	6.75

*Aged = 1023 K, 3.6 × 10^5 sec.
**Crept = 1000 K, 100 MPa, 3.5 × 10^5 sec.

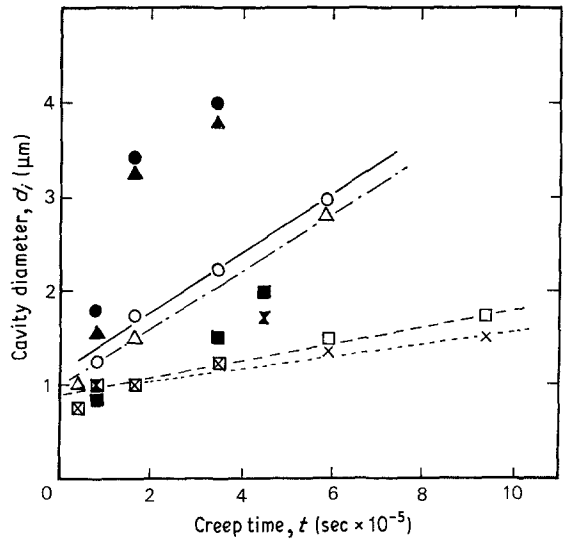

Figure 9 Variation of the diameter of the ith largest cavity with creep time in crept (1000 K, 100 MPa) specimens. Aged (open symbols) and SA (closed symbols): (○, ●) C,1; (△, ▲) S,2; (□, ■) SP,3; (×, ⧗) P,4.

the present work, the extent of cavity nucleation is evaluated as a cavity nucleation factor, P, cavity density on unit grain boundary area per 1% creep strain, which is considered only in the range of measurable cavity size, say $\geqq 0.2\,\mu m$.

As it is shown in Table II, phosphorus has been found to promote the nucleation of cavities in type 304 stainless steel: the cavity nucleation factors in the phosphorus-added steels were 4 to 5 times larger than those in the phosphorus-free steels. However, there was little difference in cavity nucleation between the sulphur-added steels and sulphur-free steels (C,1 : S,2 or SP,3 : P,4) It has also been found that prior solution annealing accelerates the cavity nucleation rate.

The effect of impurity on the cavity nucleation could be evaluated by the two different points of view. The first view is assumed to be due to the change in the size and spacing of intergranular carbides with impurity addition, which in turn alter the level of stress concentration, that is needed for cavity nucleation, through grain boundary sliding. The second is considered to be due to the impurity segregation at grain boundaries and/or cavity surfaces, which affects the interfacial energy and diffusivity, consequently, nucleation kinetics of creep cavition.

Little difference in the experimental observations for intergranular carbides with impurity addition, shown in Table IV, implies that the first view of impurity effect may be negligible in cavity nucleation. Therefore, observed impurity effect may be thought to be due to the segregation effect under the test conditions studied.

Observed effects of impurity segregation on nucleation of cavities may be explained by referring to the cavity size distribution histogram normalized by 1% creep strain as shown in Figs 7 and 8. The experimental data could be best curve fitted as

$$n_b = A/d^2 \quad m^{-2} \text{ per } 1\% \text{ creep strain} \qquad (1)$$

where n_b is the cavity density on grain boundary normal to the stress axis, A is a constant which is dependent on material and d is the cavity diameter in micrometres.

On the other hand, it is generally accepted [24] that only those cavities can be stable and grow whose size exceeds the critical diameter, d_c

$$d_c = 4\gamma_s/\sigma_n \qquad (2)$$

where γ_s is the surface energy and σ_n is the local stress normal to the grain boundary. Cavities smaller than critical size sinter up.

It is assumed that the impurity segregation at grain boundary and cavity surfaces may influence nucleation of creep cavity in the one or all of the the following three ways.

The first is that the segregation at the creep cavities reduces the surface energy, γ_s, in Equation 2. Such a reduction in surface energy of the cavity would allow a smaller stable cavity size so it is expected that the cavities would be nucleated at a higher rate than that of the alloys with lower level of segregating impurities. In the present work, however, consideration of this effect could be excluded, because those cavities whose sizes were measurable have been considered only in obtaining cavity nucleation factors.

The second is that the segregation at grain boundaries reduces the intergranular cohesion to make easier mechanical generation of cavities so that more cavities are nucleated per unit strain in the segregated boundaries. This effect is thought to result in raising cavity size distribution histogram to the higher level as it can be seen in Figs 7 and 8.

The third influence of impurity segregation arises from the segregation at the grain boundaries, which in turn reduces grain boundary diffusivity through reduction in free volume of grain boundary [25]. A slower stress relaxation rate due to a slower grain boundary diffusion, and therefore a longer duration of high stress concentration, is therefore expected to lead to a high cavity nucleation.

The AES results of crept specimen provide direct evidence for such segregation effects. Impurity effects can be deduced from the fact that phosphorus and sulphur segregation occur at both grain boundaries and cavity surfaces. Segregation of phosphorus at

TABLE V Auger peak height ratio and at % from AES results

Specimen	Description	Peak height ratio		at %	
		P/Fe	S/Fe	P	S
SP,3* (S, P-doped 304 s/s)	1. Flat grain boundary	0.15	0.02	3.89	0.26
	2. Cavity surface containing MnS inclusion	0.09	0.33	2.43	5.54
	3. Cavity surface	0.10	0.05	2.78	0.85

*Aged (1023 K, 3.6 × 10^5 sec) + Crept (1000 K, 100 MPa, 3.5 × 10^5 sec).

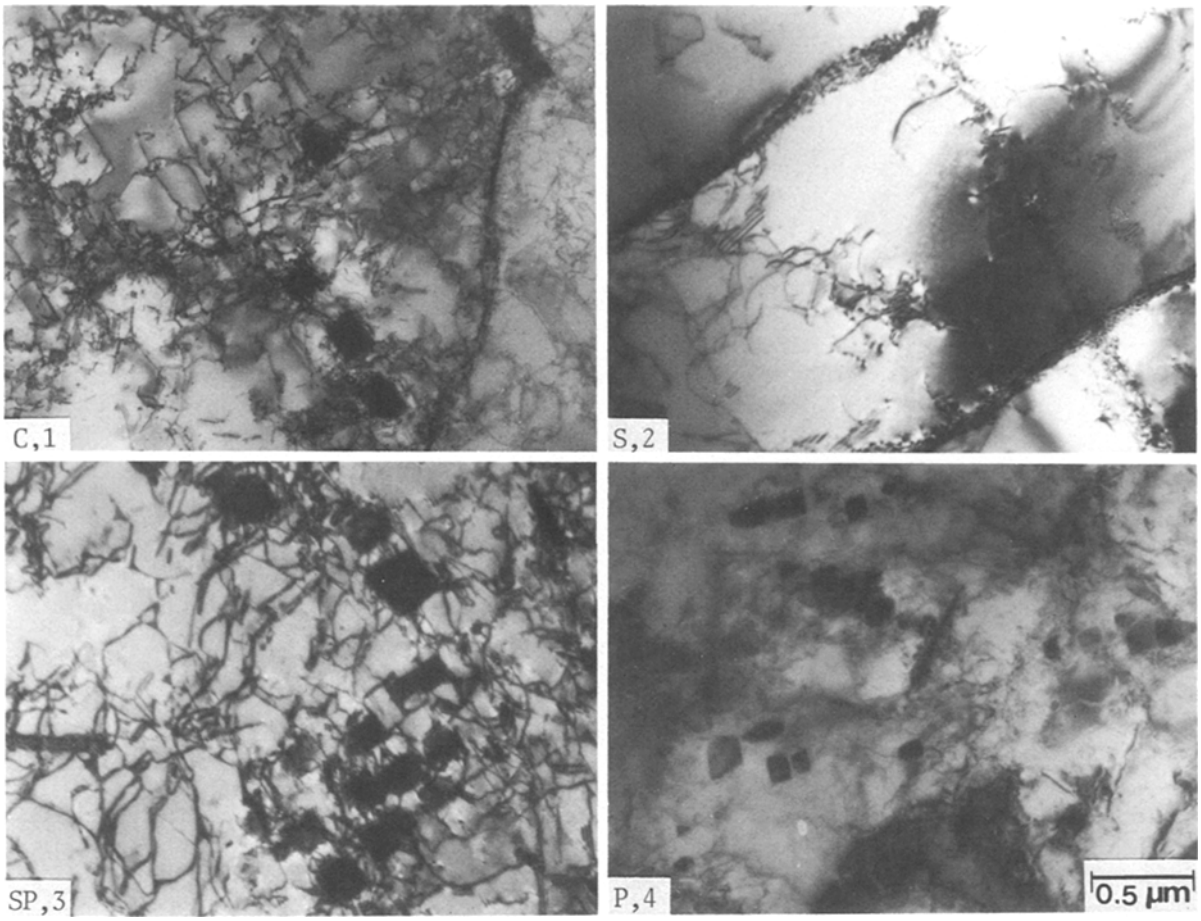

Figure 10 TEM micrograph of thin foils from aged and crept (1000 K, 100 MPa, 3.5 × 10^5 sec) samples.

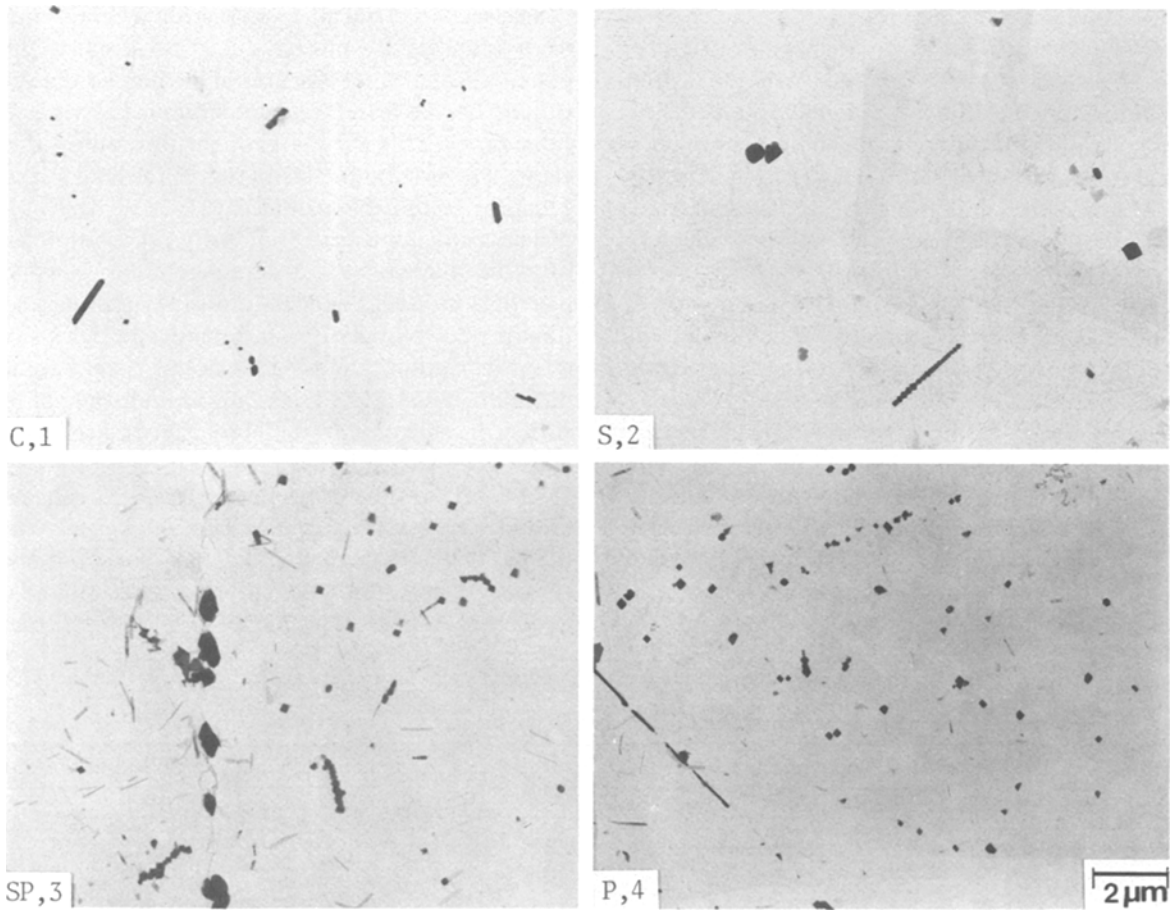

Figure 11 TEM micrograph of carbon extraction replicas from aged and crept (1000 K, 100 MPa, 3.5 × 10^5 sec) samples.

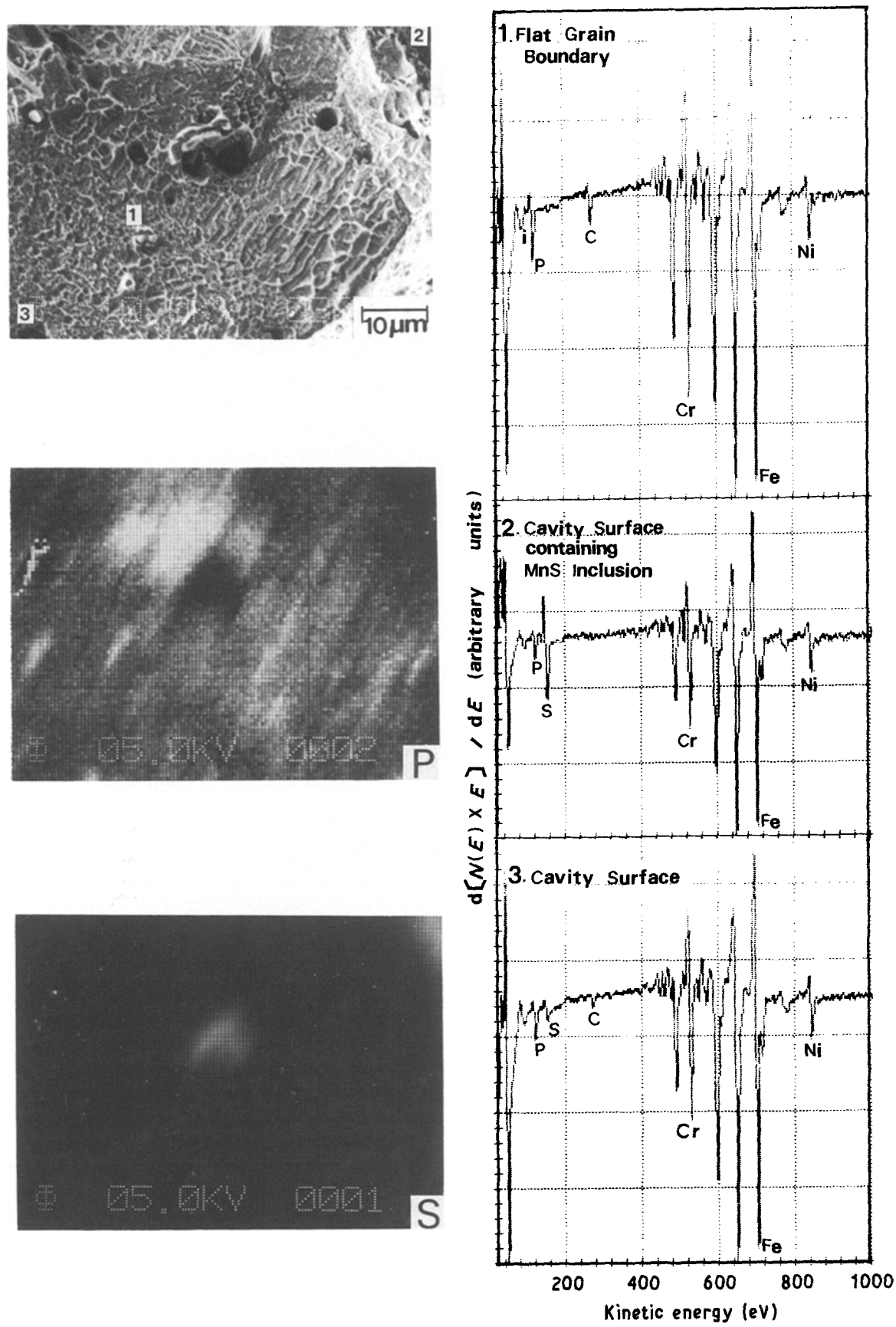

Figure 12 AES secondary electron image, corresponding Auger maps for phosphorus, sulphur and Auger spectra in SP,3 specimen aged and crept at 1000 K, 100 MPa for 3.5×10^5 sec.

grain boundary is more intense than that of sulphur, while sulphur, while sulphur segregates at cavity surfaces more intensely than at grain boundaries as indicated in Fig. 12.

In this work, however, the experimental evidence shows that the above mentioned impurity effects are only applicable to phosphorus. Sulphur is observed to be an impurity which gives little effect on cavity nucleation. Although more MnS inclusions have also been observed on grain boundaries in sulphur-added steels than in sulphur-free steels, the effects of sulphur on cavitation have not been detected.

Generally, sulphur is known to be the overwhelming segregation element, which acts through selective

segregation at internal free surface where it can play a key role on cavitation in nickel, nickel-base superalloys [26, 27] and ferritic steels [5]. In the steels studied, on the contrary, the effects of sulphur may be scavanged by relatively high manganese contents of $\sim 0.9\%$. Further research is needed to determine what is the significance of sulphur with respect to cavitation.

On the other hand, slight acceleration in nucleation for prior solution annealed steels can be explained as the following. For steels in solution annealed condition prior to testing, intergranular carbides form continuously during creep, thereby providing a continuous supply of sites at which cavities can nucleate. High tendency to cavitation can be expected in the solution annealed steels from high stress concentration by grain boundary sliding due to the small and non-continuous carbides precipitated at boundaries as shown in Table IV.

With the information available it is not fair to decide which of the mechanisms is responsible for the observed cavitation in the present work. However, it would appear that vacancy condensation mechanism can explain impurity effects on nucleation of cavity. Therefore vacancy condensation mechanism can be assumed to be significant under the test conditions studied.

4.2. Impurity effects on cavity growth

As is shown in Fig. 9 and Table III, phosphorus shows apparent effect in retarding the growth rate of creep cavities by 4 to 5 times. Sulphur, on the other hand, has little effect. Solution annealing prior to testing also causes an increase in the cavity growth rate by 2 to 3 times more than ageing does.

As is discussed in Section 4.1 of cavity nucleation, almost the same analysis can be applied for impurity effects on cavity growth.

Phosphorus effects on cavity growth could be assessed by considering segregation at grain boundaries, and thereby reducing grain boundary diffusivity. The AES results of Fig. 12 confirm that phosphorus segregates strongly at grain boundaries. Reduction in grain boundary diffusivity due to impurity segregation can be also analogized from the limited data on other alloys [28] and from the phenomenological relationship of Borisov *et al.* [29]. The greater reduction of grain boundary diffusivity, due to a higher phosphorus segregation level in phosphorus-added steels, makes the cavities grow slowly under the assumption of grain boundary diffusion controlled cavity growth. Good agreement between measured and calculated growth rates supports the assumption.

On the other hand, sulphur and prior ageing effects can be explained by similar ways as discussed in nucleation of cavities. Acceleration in growth rate for prior solution annealing can be attributed to the easy cavity nucleation, thereby shortening cavity spacing, due to the condition of intergranular carbides.

5. Conclusions

1. The segregation of phosphorus and sulphur at grain boundaries and creep cavities have been observed in crept specimens. Segregation of phosphorus was more extensive at grain boundaries than at cavity surfaces, whereas sulphur was vice versa.

2. Phosphorus accelerates the nucleation of creep cavities, but retards the growth of them.

3. Sulphur has little effect on creep cavitation.

4. Ageing prior to testing inhibits the nucleation and growth of creep cavities.

Acknowledgement

The authors wish to thank Professor Jin Yu of KAIST for many useful discussions during this work. We also wish to express our gratitude to Dr J. J. Yi of POSCO for AES investigations.

References

1. C. L. BRIANT and S. K. BANERJI, *Metall. Trans.* **12A** (1981) 309.
2. J. KÜPPER, H. ERHART and H. J. GRABKE, *Corr. Sci.* **21** (1981) 227.
3. K. YOSHINO and C. J. McMAHON Jr, *Metall. Trans.* **5A** (1974) 363.
4. H. R. TIPLER and B. E. HOPKINS, *Met. Sci.* **10** (1976) 47.
5. S. H. CHEN, T. TAKASUGI and D. P. POPE, *Metall. Trans.* **14A** (1983) 571.
6. R. W. SWINDEMAN, V. D. SIKKA and R. L. KLUEH, *ibid.* **14A** (1983) 581.
7. R. VISWANATHAN, *ibid.* **6A** (1975) 1135.
8. M. P. SEAH, *Phil. Trans. R. Soc. A* **295** (1980) 265.
9. H. R. TIPLER and D. McLEAN, *Met. Sci.* **4** (1970) 103.
10. W. D. NIX, K. S. YU and J. S. WANG, *Metall. Trans.* **14A** (1983) 563.
11. D. GUPTA, *ibid.* **8A** (1977) 1431.
12. W. LOSCH and I. ANDREONI, *Scripta Metall.* **12** (1978) 277.
13. S. DANYLUK, I. WOLKE, J. H. HONG and E. A. LORIA, *J. Mater. Energy Syst.* **7** (1985) 6.
14. J. L. BRIMHALL, D. R. BAER and R. H. JONES, *J. Nucl. Mater.* **117** (1983) 218.
15. *Idem, ibid.* **122/123** (1984) 196.
16. L. E. DAVIS, N. C. McDONALD, P. W. PALMBERG, G. E. RIACH and R. E. WEBER, in "Handbook of Auger Electron Spectroscopy" (Physical Electronics Industries, Eden Prairie, MN, 1976) p. 1.
17. E. D. HYAM, in "Structural Processes in Creep" (Iron and Steel Institute, London, 1961) p. 76.
18. N. G. NEEDHAM and T. GLADMAN, *Met. Sci.* **14** (1980) 64.
19. B. J. CANE and G. W. GREENWOOD, *ibid.* **9** (1975) 55.
20. D. A. MILLER, F. A. MOHAMED and T. G. LANGDON, *Mat. Sci. Eng.* **40** (1979) 159.
21. G. R. KEGG, J. M. SILCOCK and D. R. F. WEST, *Met. Sci.* **8** (1974) 337.
22. B. R. BANERJEE, E. J. DULIS and J. J. HAUSER, *Trans. ASM* **61** (1968) 103.
23. J. P. SHEPHERD, *Met. Sci.* **10** (1976) 174.
24. R. RAJ, *Acta Metall.* **26** (1978) 995.
25. J. BERNADINI, P. GAS, E. D. HONDROS and M. P. SEAH, *Proc. R. Soc. A* **379** (1982) 159.
26. W. C. JOHNSON, J. E. DOHERTY, B. H. KEAR and A. F. GIAMEI, *Scripta Metall.* **8** (1974) 971.
27. R. T. HOLT and W. WALLACE, *Int. Met. Rev.* **21** (1976) 1.
28. E. D. HONDROS, *Proc. R. Soc. A* **286** (1965) 479.
29. V. T. BORISOV, V. M. GOLOKOV and G. V. SCHERBENDINSKY, *Fiz. Met. Metalloved* **17** (1964) 881.

Received 27 November 1985
and accepted 21 January 1986